Project report for SCEC Award 16061: "Effect of geothermal operations on earthquake source processes in the Salton Sea geothermal field"

Xiaowei Chen
Department of Geology and Geophysics, the University of Oklahoma.

Abstract:

The borehole network operated by CalEnergy provides high quality dataset for the microearthquakes in the Salton Sea geothermal region. The network was open to public from 2008 to early 2014, which recorded over 7000 earthquakes in the geothermal field. We obtain high-resolution earthquake locations for the Salton Sea Geothermal field with seismic data recorded by a local borehole network and a 3D velocity model. Previous analysis of seismicity clustering leads to the unique spatial distribution and characteristics of the "mixture-type" cluster, which is predominately located within active injection areas, differs from the traditional "aftershock-type" or "swarm-type" clusters. Analysis in this report is focused on spectral analysis using a stacking approach to understand the spatial distributions of stress drop, and the relationship with injection/production wells. The results suggest there exist coherent spatial patterns of stress drop distribution, and seismicity characteristics. We also perform relative-stress drop analysis for a tight repeating earthquake cluster. The relative stress drop confirms the variability of stress drop distributions from stacking analysis.

Intellectual merit:

The research contributes to integrated understanding of the geomechanical process within the active geothermal field. The analysis of the spatial distributions of earthquake stress drop will provide key information for hazard assessment. The comparison between stacking approach and relative individual pair analysis provide constraints for the reliability and stability of source parameter estimations.

Broader impacts:

The project results are beneficial for learning earthquake hazards, risks and earthquake physics. Due to the recent increase in earthquakes in central US, the students at the University of Oklahoma are interested in learning more about induced seismicity, and enrolled in my seminar on "induced seismicity". Student Yifang Cheng at OU has been working on this project since Jan 2015. She has completed her master thesis in summer 2016, and now a PhD student at USC.

Technical report:

1. Project objective:

We plan to use the Borehole network deployed by CalEnergy with open access data from 2008 to 2014, to investigate detailed spatial and temporal variations of earthquake stress drop within the three small clusters defined by geothermal injection/production well locations. With these results, we would like to address:

(1) Are there temporal changes in earthquake source spectra in response to different stages of geothermal operation? Are these variations link to fluid pressure variations due to changes in operation?

(2) What is the spatial influence window of the geothermal injection activities? Is there potential to trigger larger events in this area?
(3) Are there differences in earthquake responses among the three clusters in response to different injection parameters?

2. Research progress

Data and catalog

We download triggered waveforms archived in the Southern California Earthquake Data Center (SCEDC) and organize the waveforms into an event-based file system. Because of missing S-wave picks on the borehole network, an auto-picker algorithm (Jeff McGuire, personal communication) is applied to obtain more complete S-wave arrivals. We then measure more precise differential times using waveform cross-correlation with sub-sample accuracy of 0.001s between 2 and 10 Hz. The correlation coefficients are measured for each earthquake with the nearest 500 earthquakes, using time windows of -0.3s before and 0.8s after P-wave arrivals, -0.5s before and 1.0s after S-wave arrivals. Only pairs with cross-correlation coefficients > 0.8 are included. Over 1 million absolute and differential arrival times for 7348 earthquakes are included in double-difference relocation using tomoDD package [*Zhang and Thurber*, 2003], based on the 3D velocity model [*Mcguire et al.*, 2015]. Specifically, we use 431,872 catalog P differential times, 282,933 catalog S differential times, 819,649 cross-correlation P differential times, and 752,157 cross-correlation S differential times. The relative location uncertainty is estimated to be 51 m in horizontal direction and 41 m in depth using a bootstrap resampling approach. Final earthquake locations are more tightly clustered than the original catalog locations. The locations clearly illuminates the three sub-clusters in the geothermal field, which corresponds to three groups of injection wells [*Chen and Shearer*, 2011]. Most events are located between 2 and 5 km. For the middle sub-cluster, most larger ($M > 2.5$) events are located at shallow depth, and a microearthquake cloud that clearly lacks any larger events occurs between 3 and 5 km depth.

Spectral analysis:

For spectral analysis, we compute displacement spectra of short period instruments using the multitaper method of *Prieto et al.*, [2009] using a 0.5 s time windows before (noise) and after (signal) the picked P and S arrivals. We require a signal-to-noise (STN) amplitude ratio of at least 3 between 3-15 Hz frequency bands and 2 between 15-20 Hz for all spectra for the analysis (note that the STN requirement is comparable to *Chen and Shearer* [2011], where average STN of 5 is required for each frequency bands), and also require each event to be recorded at this signal-to-noise level by at least five different stations. This restriction is intended both to better isolate station effects, and to average out directivity effects, which can affect the source parameter estimation [*Venkataraman and Kanamori*, 2004].

We first apply the method in *Shearer et al.*, [2006] to compute an empirical correction spectrum for each of the sub-areas. The areas are divided based on spatial clustering of the seismicity. The central field is divided into areas 1 and 2 based on the

depth distribution – area 1 is primarily at shallower depth, and area 2 is at deeper depths. For each of the sub-areas, we obtain the stress drop for individual earthquakes.

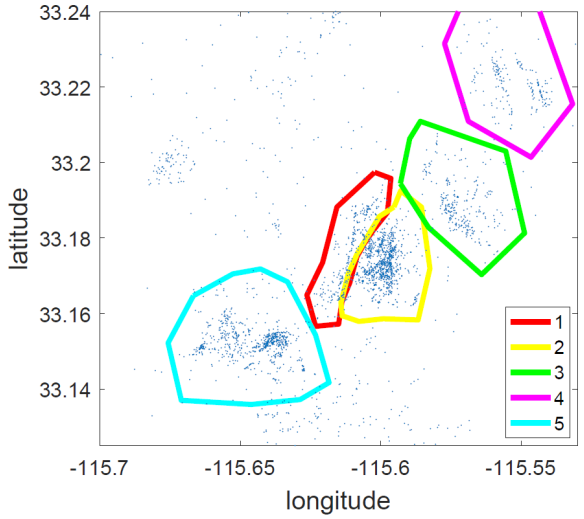

Figure 1. Selected regions for stress drop estimation. For each region, I compute a single Empirical Green's Function (EGF) computed from the stacked the events spectra terms and use it to correct spectra.

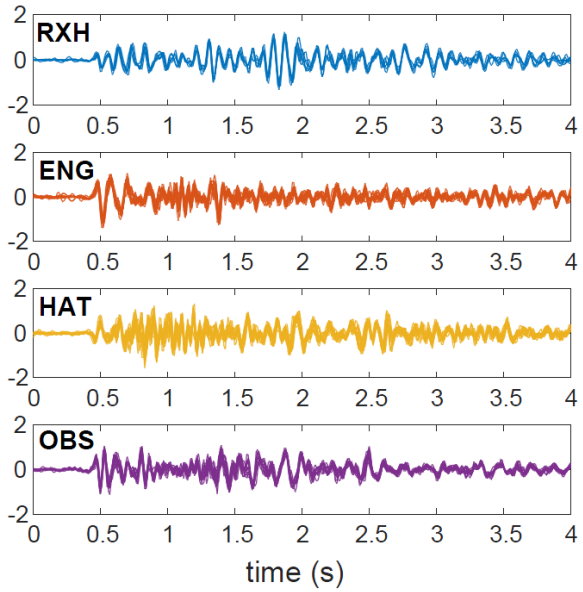

Figure 2. Normalized waveform for the 15 events in the repeating cluster recorded at four different borehole stations.

Overall, the median stress drop is 0.3 MPa, with standard deviation in log10 domain of 0.6, consistent with previous analysis in *Chen and Shearer* [2011]. However, the new results have higher spatial resolution with the middle geothermal field (areas 1 and 2), where most the seismicity occurred during the study period. The higher spatial resolution allows detailed analysis of the relationship between earthquake source parameters and seismicity characteristics (further discussion).

To further validate the observed stress drop variability, we search for "repeating" earthquake cluster with correlation coefficients > 0.9 at minimum of two stations between 10 to 40 Hz. We identify a repeating cluster with 15 events with magnitudes ranging from 0.5 to 1.7, and show striking similarity across the borehole network. Figure 2 shows the normalized waveform for all 15 events at four borehole stations. These events are located within a tight cluster spanning about 100 m radius in the microseismicity cloud (i.e., the area with mixture-type clustering). The high level of similarity at high frequency suggests similar frequency contents (and similar corner frequency) of the spectra. However, the wide range of magnitude suggests that the stress drops for these events may differ.

For the 15 events, we apply a method to analyze the relative source dimension, stress drop ratio and magnitude ratio following *Lengliné et al.*, [2014]. The source dimension exhibits relatively small variability, ranging from 62m to 82m based on the relationship between corner frequency and source dimension, assuming a circular rupture model. The similar source dimension but different magnitudes translates into high stress drop variability: relative stress drop range from 1

to 25 when compared with a reference event. The relative source parameter estimations confirm the observed stress drop variability from the stacking approach. The highly variable stress drop is likely caused frequent stress perturbation from fluid injection that reduces normal stress on the asperity.

Interpretation:

The highlight of our research is the coherent spatial distributions between stress drop and seismicity. Focusing on the middle field, areas with low b-value at shallow depth are characterized with high stress drop. At middle depth range of about 4 km, it is dominated by mixture-type clustering, high b-value and low stress drop. Figure 3 reveals gradual spatial transition from low b-value to high b-values following the transition from 400°C near the injection wells, to 800°C near the production wells in the middle of profile DD'. The b-value gradually decreases moving further north away from the 800°C gradient area. The stress drop and clustering show similar patterns in the spatial transition. Both the stress drop and b-value distributions are opposite to typically observed depth-dependence, where stress drop tends to increase with depth, and b-value tends to decrease with depth. The agreement between the coherent spatial patterns of seismicity and source parameters suggests there exist common physical control of seismicity characteristics and rupture processes. We interpret the characteristics as a result of frequent fluid circulation, temperature variations, variations of fracture density in relation to the intrusion body. The tomographic imaging from *McGuire et al.,* [2015] suggests that most earthquakes occur in high-temperature, high Vp regions. The high Vp is primarily due to the metamorphic process at shallower depth.

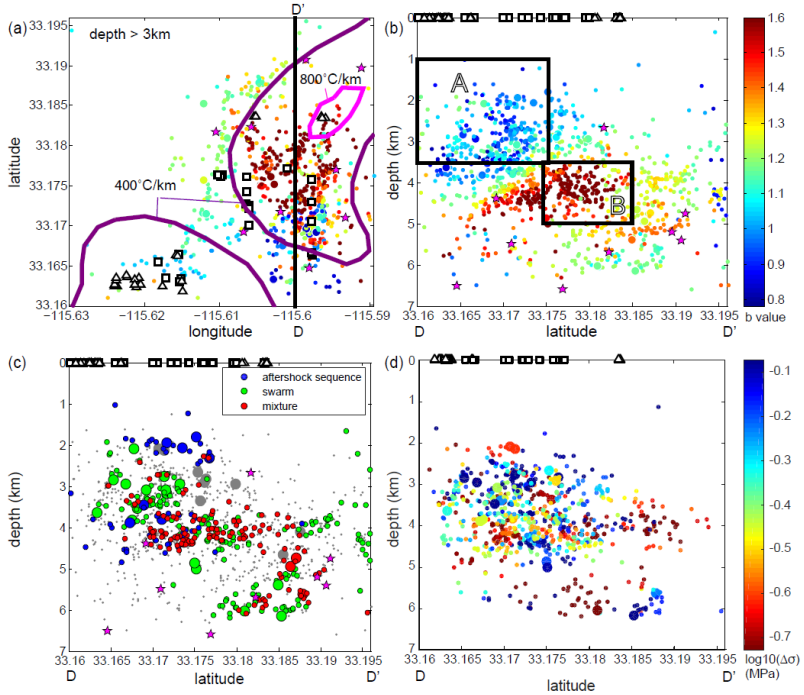

Figure 3. *B*-value, cluster-type, and stress drop distributions within the middle cluster. (a) Map view of *b*-value distributions (for clarity reasons, only events >3 km are plotted), and contour lines of 800°C/km and 400°C/km geothermal gradient. (b) Cross-section view of *b*-value along DD' profile (latitude versus depth). For both (a) and (b), events are colored with *b*-value. (c) Cross-section view of clustering type along DD' profile (latitude versus depth). Events within clusters are colored according to clustering type, non-clustered events are shown in grey dots. (d) Cross-section view of stress drop variation along DD' profile (latitude versus depth). Events are colored by the median stress drops of their nearest 10 events. Injections wells are white squares, and productions wells are white triangles. Historic large magnitude events with $M_L \geq 4$ since 1981 are plotted by magenta star.

A further question remains is that whether injection or production activities are more likely associated with the microseismicity cloud. Figure 3 shows the gradual transition of earthquake characteristics from the injection wells (to the south) to the production wells (to the north), and the microseismicity cloud (near the mixture type in Figure 3c) is primarily located beneath a few injection wells. We further analyze the relationship between earthquake frequency and injection/production wells. Figure 4a shows that high concentration of microearthquakes within 0.5 km of injection wells, which is less prominent for production wells – high density spreads between 0.2 and 1.5 km. This suggests that the microseismicity cloud is primarily associated with injection well. This is consistent with the interpretation of the highly variable stress drop for a repeating cluster within the microseismicity cloud. Both Figure 4a and 4b show that the earthquakes can be naturally divided into two groups based on the distance to wells, further supports the previous observations of the difference in earthquake clustering inside and outside the geothermal field. It should be noted that this analysis is only made possible with a lower Mc between 2008 and 2014 (~0.6) – if a higher Mc had been used (e.g., M>1.5), then the difference between injection and production wells would be relatively difficult to identify.

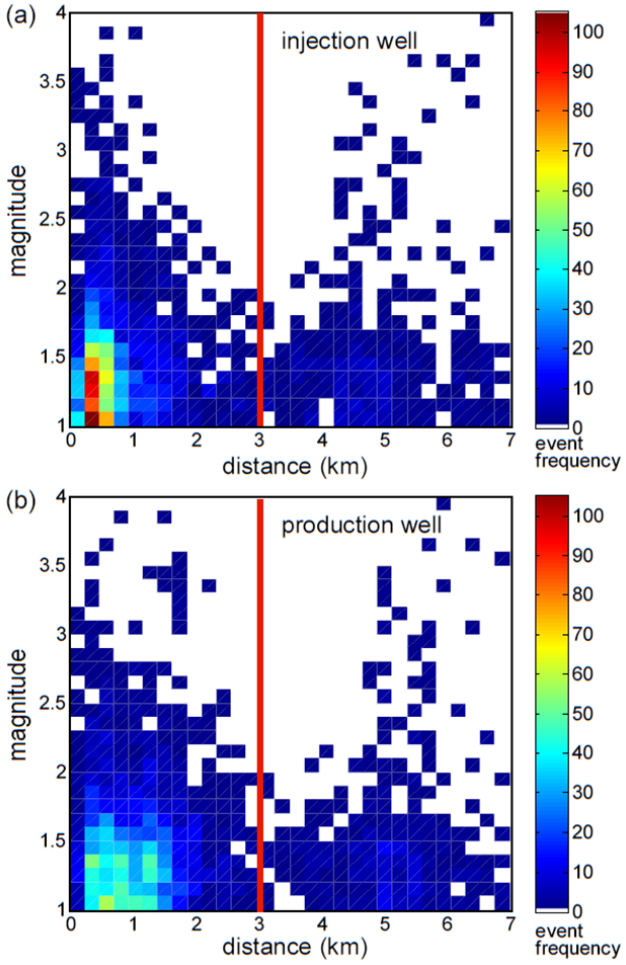

Figure 4. 2D histogram of event density per magnitude and distance relative to nearest (a) injection wells and (b) production wells. The events can be clearly divided into two groups depending on the distance to nearest well (red line).

Presentations and publications:

Student Yifang Cheng presented her result at SCEC and AGU 2016, she has completed her master thesis in summer 2016, and two manuscripts for seismicity and source spectra. She also presented her research at student symposium at OU, and won the best poster award for master students.

Reference:

Chen, X., and P. M. Shearer (2011), Comprehensive analysis of earthquake source spectra and swarms in

the Salton Trough, California, *J. Geophys. Res.*, *116*(B09309), doi:10.1029/2011JB008263.

Lengliné, O., L. Lamourette, L. Vivin, N. Cuenot, and J. Schmittbuhl (2014), Fluid-induced earthquakes with variable stress drop, *Joural Geophys. Res.*, *119*, 8900–8913, doi:10.1002/2014JB011282.

Mcguire, J. J., R. B. Lohman, R. D. Catchings, M. J. Rymer, and M. R. Goldman (2015), Relationships among seismic veloicty, metamorphism, and seismic and aseismic fault slip in the Salton Sea Geothermal Field region, *J. Geophys. Res. Solid Earth*, *120*, 2600–2615, doi:10.1002/2014JB011579.

Prieto, G. A., R. L. Parker, and F. L. Vernon III (2009), A fortran 90 library for multitaper spectrum analysis, *Comput. Geosci.*, *35*, 1701–1710.

Shearer, P. M., G. A. Prieto, and E. Hauksson (2006), Comprehensive analysis of earthquake spectral in southern California, *J. Geophys. Res. Earth*, *111*(B6), doi:B0630310.1029/2005jb003979.

Venkataraman, A., and H. Kanamori (2004), Observational constraints on the fracture energy of subduction zone earthquakes, *J. Geophys. Res.*, *109*(B05302), doi:10.1029/2003JB002549.

Zhang, H., and C. H. Thurber (2003), Double-difference tomography: The method and its application to the Hayward Fault, California, *Bull. Seismol. Soc. Am.*, *93*(5), 1875–1889, doi:10.1785/0120020190.